SciEn
Proceedings of 8th International Conference on Mechanical Engineering and Renewable Energy 2025
10-12 December, 2025, Chattogram, BANGLADESH
SciEn Conference Series: Engineering Vol. 4, 2026, pp 247-252 https://doi.org/10.38032/scse.2026.4.119

Effects of Inclined Magnetic Field and Higher-Order Velocity Slip on Boundary Layer Casson Nanofluid Flow over a Stretching Sheet

Umme Hani[1], Mohammad Ali[1,], Muhammad Shahnewaz Bhuyan[1], Rehena Nasrin[2]*

[1]Department of Mathematics, Chittagong University of Engineering & Technology, Chattogram-4349, Bangladesh
[2]Department of Mathematics, Bangladesh University of Engineering and Technology, Dhaka, Bangladesh

ABSTRACT

This paper investigates how higher-order velocity slip affects the flow of Casson nanofluid over a stretched sheet within the boundary layer (BL), considering an inclined magnetic field and the Buongiorno model. The similarity transformation is used to convert a collection of ordinary differential equations into a collection of partial differential equations. The Spectral Quasi-linearization approach is used to solve the modeled system numerically and examine how various fluid parameters affect the temperature, concentration, and velocity profiles. The findings of the important physical characteristics have been depicted graphically. It is observed that velocity reduces but temperature enhances for an increment of magnetic field parameter, inclination angle, Casson parameter, and first-order velocity slip parameter. Also, concentration increases close to the sheet but declines far from the sheet for larger values of Brownian motion parameter and Schmidt number. From an MHD flow and heat transfer perspective, numerous engineering applications can benefit, including petroleum processing, MHD power generation, aerodynamic boundary layer control, polymer sheet production, glass fiber manufacturing, and many others.

Keywords: Casson Nanofluid; Inclined Magnetic Field; Brownian Motion; Thermophoresis; Higher-Order Velocity Slip.

1. Introduction

Papers Boundary layer (BL) flow across a stretched sheet is a significant issue in various industrial applications, including paper production, and elastic sheets. In order to model fluid flow, Ludwig Prandtl first put out boundary layer hypothesis in 1904 [1]. Based on the governing equations of BL flow through a continuously intensifying surface moving at fixed velocity, the innovative contribution in this field was introduced by Sakiadis [2]. Bakar et al. [3] explored the stable laminar flow in the boundary layer over a stretched sheet with partial slip, incorporating a convective surface boundary condition (BC). Vinod et al. [4] conducted a detailed investigation of the MHD BL flow and heat transfer characteristics of a Casson fluid through an exponentially stretched sheet, incorporating the influences of thermal radiation and heat source/sink.

Nanofluids can serve as effective heat exchange fluids, using a range of approaches to improve their performance because of their improved thermophysical properties. Gladys and Reddy [5] investigated how the fluid thermal conductivity of nanoparticles was enhanced. A jet cooling flow of nanofluid and heat transference on a heat surface with different levels of roughness were investigated by Priya G. et al. [6].

Casson fluid, a fascinating non-Newtonian liquid, is becoming increasingly important in our daily lives. Everyday foods like sauces, soups, and jellies are perfect examples of Casson fluids. The modeling equations for Casson fluids were first developed by Casson [7] in 1959, who also demonstrated the distinct properties of several polymers. Shekar and colleagues [8] concentrated on investigating the impacts of the Casson and chemical reaction parameters on the changing radiative flow of MHD Nanofluid over a sheet that was stretched. Hussain et al. [9] considered the Buongiorno model to investigate the mixed convection BL flow of a Casson nanofluid on an exponentially stretched sheet with an internal heat source. Sekhar et al. [10] examined magnetohydrodynamic Casson nanofluid flow over an inclined stretching surface, accounting for Soret–Dufour, thermal radiation, and heat sources/sinks effects.

The effect of the magnetic field plays a crucial role in MHD generators, bearings, pumps, and other devices, particularly in boundary layer control, where it interacts with electrically conducting fluids. Vijayalaxmi and Shankar [11] examined Casson nanofluid flow over a nonlinear stretching sheet under the effects of an inclined magnetic field, chemical reactions, and second-order thermal, velocity, and solutal slips. The importance of examining how the Casson fluid behaves when exposed to an electrically conducting and stretching sheet while taking into account the effects of chemical reactions, viscous dissipation, an aligned magnetic field was discussed by Kosar et al. [12].

To the best of knowledge, not much study has been done on Casson nanofluid across stretching surfaces while accounting for higher order velocity slip and an angled magnetic field. So, motivated by the foregoing explanation, the current research focus on the effects of higher-order velocity slip and angled magnetic field on Casson nanofluid flow over a stretched sheet in the boundary layer.

2. Mathematical Formulation

The current model takes higher-order velocity slip into account while examining the incompressible, 2-dimensional,

*Corresponding Author Email Address: ali.mehidi93@gmail.com

and steady Casson nanofluid flow through a linearly stretched sheet. The strength magnetic field is applied along y-axis perpendicularly with an acute angle γ. Let $u_w = ax$ be the stretching velocity, and $U = bx$ be the free stream velocity (a and b are the positive constants). It is assumed that Tw, Cw, T∞, and C∞ stand for the temperature and concentration at the surface, ambient fluid temperature, and concentration of the Casson nanofluid, respectively.

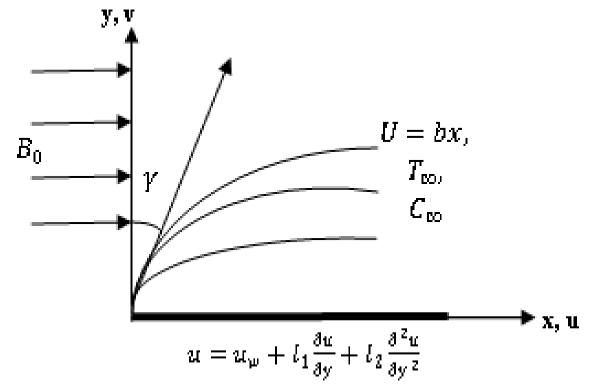

Fig.1: Flow configuration

Using the aforementioned assumption, the governing equations are the following according to Srinivasulu and Goud [13]:

$$\frac{\partial u}{\partial x} + \frac{\partial v}{\partial y} = 0; \quad (1)$$

$$u\frac{\partial u}{\partial x} + v\frac{\partial u}{\partial y} = \nu\left(1+\frac{1}{\beta}\right)\frac{\partial^2 u}{\partial y^2} - \frac{\sigma B_0^2}{\rho_f}\gamma\ ; \quad (2)$$

$$u\frac{\partial T}{\partial x} + v\frac{\partial T}{\partial y} = \alpha\frac{\partial^2 T}{\partial y^2} + \tau\left[D_B\frac{\partial T}{\partial y}\frac{\partial C}{\partial y} + \frac{D_T}{T_\infty}\left(\frac{\partial T}{\partial y}\right)^2\right]; \quad (3)$$

$$u\frac{\partial C}{\partial x} + v\frac{\partial C}{\partial y} = D_B\frac{\partial^2 C}{\partial y^2} + \frac{D_T}{T_\infty}\frac{\partial^2 T}{\partial y^2}; \quad (4)$$

The boundary conditions are

$$u = u_w + l_1\frac{\partial u}{\partial y} + l_2\frac{\partial^2 u}{\partial y^2}, -k\frac{\partial T}{\partial y} = h_f(T_f - T), D_B\frac{\partial C}{\partial y} + \frac{D_T}{T_\infty}\frac{\partial T}{\partial y} = 0 \quad \text{at} \quad y = 0 \quad (5)$$

$$u \to U, T \to T_\infty, C \to C_\infty \quad \text{at} \quad y \to \infty \quad (6)$$

Introducing the following similarity transformation as

$$\eta = y\sqrt{\frac{a}{\nu}}, \psi = \sqrt{a\nu x}f(\eta), \theta(\eta) = \frac{T-T_\infty}{T_f-T_\infty}, \phi(\eta) = \frac{C-C_\infty}{C_f-C_\infty} \quad (7)$$

After using Eq. (7), the reducing form of Eqs. (2), (3), and (4) can be written as

$$\left(1+\frac{1}{\beta}\right)f''' + ff'' - f'^2 - Mf'\gamma\ = 0; \quad (8)$$

$$\theta' + Pr(f\theta' + Nb\theta'\phi' + Nt\theta'^2) = 0; \quad (9)$$

$$\phi' + Scf\phi' + \frac{Nt}{Nb}\theta'' = 0; \quad (10)$$

With the corresponding boundary conditions

$$f = 0, f' = 1 + \delta_1 f'' + \delta_2 f''', \theta' = Bi(\theta - 1), Nb\phi' + Nt\theta' = 0 \quad \text{at} \quad \eta = 0 \quad (11)$$

$$f' \to A, \theta \to 0, \phi \to 0 \quad \text{at} \quad \eta \to \infty \quad (12)$$

In above Eqs. $M = \frac{\sigma B_0^2}{\rho_f a}, Nb = \frac{\tau D_B(C_f - C_{=})}{\nu}, Sc = \frac{\nu}{D_B},\ Nt = \frac{\tau D_T(T_f - T_\infty)}{T_\infty \nu},\ \delta_1 = l_1\sqrt{\frac{a}{\nu}},\ Pr = \frac{\nu}{\alpha}\ , \delta_2 = l_2\frac{a}{\nu},\ A = \frac{b}{a}, Bi = \frac{h_f}{k}\sqrt{\frac{\nu}{a}}$ represent Magnetic field parameter, Brownian motion parameter, Schmidt number, thermophoresis parameter, first-order slip parameter, Prandtl number, second-order slip parameter, stretching ratio parameter, and Biot number, respectively.

The skin friction coefficient(C_f), Nusselt number(Nu), and Sherwood number (Sh) can be defined as

$$C_f = -\frac{\mu_f}{\rho u_w^2}\left(\frac{\partial u}{\partial y}\right)_{y=0}, Nu = -\frac{xk}{k_f(T_f - T_\infty)}\left(\frac{\partial T}{\partial y}\right)_{y=0}, \text{ and } Sh = -\frac{xD_B}{D_B(C_f - C_\infty)}\left(\frac{\partial C}{\partial y}\right)_{y=0} \quad (13)$$

After putting Eq. (7) into Eq. (13), the terms that are obtained $C_f\sqrt{Re} = -\left(1+\frac{1}{\beta}\right)f''(0)$, $\frac{Nu}{\sqrt{Re}} = -\theta'(0)$, and $\frac{Sh}{\sqrt{Re}} = -\phi'(0)$.

Here $Re = \frac{u_w x}{\nu}$ is the Reynold's number.

3. Solution Procedure

It is hard to solve a nonlinear coupled ODE accurately using analytical techniques. Thus, the estimated results are computed using the numerical solver that is built into MATLAB. First, Eqs. (8) – (10) with BCs represented in Eqs. (11) & (12) are reduced to a first-order system and the bvp4c solver method is then written to determine the final fallout. The entire process is shown below:

$$(y_1, y_2, y_3, y_4, y_5, y_6, y_7)^T = (f, f', f'', \theta, \theta', \phi, \phi')$$

$$y_3' = \left(1+\frac{1}{\beta}\right)^{-1}(-y_1y_3 + y_2^2 + My_2\gamma\ ); \quad (14)$$

$$y_5' = -Pr(y_1y_5 + Nby_5y_7 + Nty_5^2); \quad (15)$$

$$y_7' = -Scy_1y_7 + \frac{Nt}{Nb}Pr(y_1y_5 + Nby_5y_7 + Nty_5^2); \quad (16)$$

$$y_2 = 1 + \delta_1 y_3 + \delta_2 y_3', y_1 = 0, y_5 = Bi(y_4 - 1), Nby_7 + Nty_5 = 0 \quad \text{at} \quad \eta = 0 \quad (17)$$

$$y_2 \to A, y_4 \to 0, y_6 \to 0 \quad \text{at} \quad \eta \to \infty\ . \quad (18)$$

4. Results and Discussion

The foremost focus of this segment is on how diverse physical parameters affect the velocity (f') temperature (θ), and concentration (ϕ) profiles. The graphs and tabular results are calculated and displayed based on the various values of dimensionless numbers such as, Magnetic field parameter, Brownian motion parameter, stretching ratio parameter, thermophoresis parameter, Schmidt number, first-order slip parameter, Prandtl number, second-order slip parameter, and Biot number for the previously described physical quantities.

Figures 2 & 3 exhibit the f', θ, and ϕ profiles for diverse values of M and γ, respectively. In Figs. 2(a) & 3(a), the velocity reduces for an increment in M and γ. It results from the Lorentz force, which is the force that resists the fluid's motion. Since M is directly proportional to $\sin^2\gamma$, it is also demonstrated that when $\gamma = 0^\circ$, the magnetic field has no effect on velocity curves, but when $\gamma = 90^\circ$, the magnetic field affects the flow. On the other hand, temperature and concentration increase for increasing values of M and γ, which are depicted in Fig. 2(b), 2(c), 3(b), and 3(c).

Electrical power is transformed into heat as a result of Lorentz force, which increase the fluid's heat and mass. The overall fluid temperature rises close to the surface of an inclined surface as the angle increases because the convective heat transfer coefficient decreases. Since convection and flow patterns alter the diffusion and movement of species within the fluid, an upsurge in the inclination angle results an increment of concentration profile.

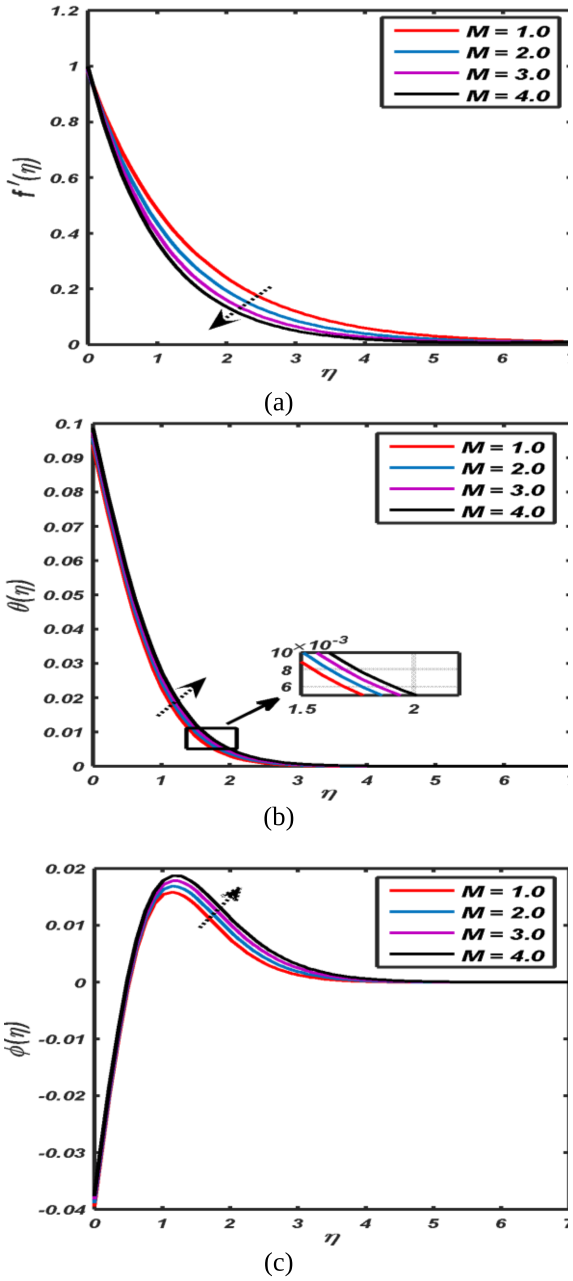

Fig.2: Variation of M on (a) f', (b) θ, and (c) ϕ profiles.

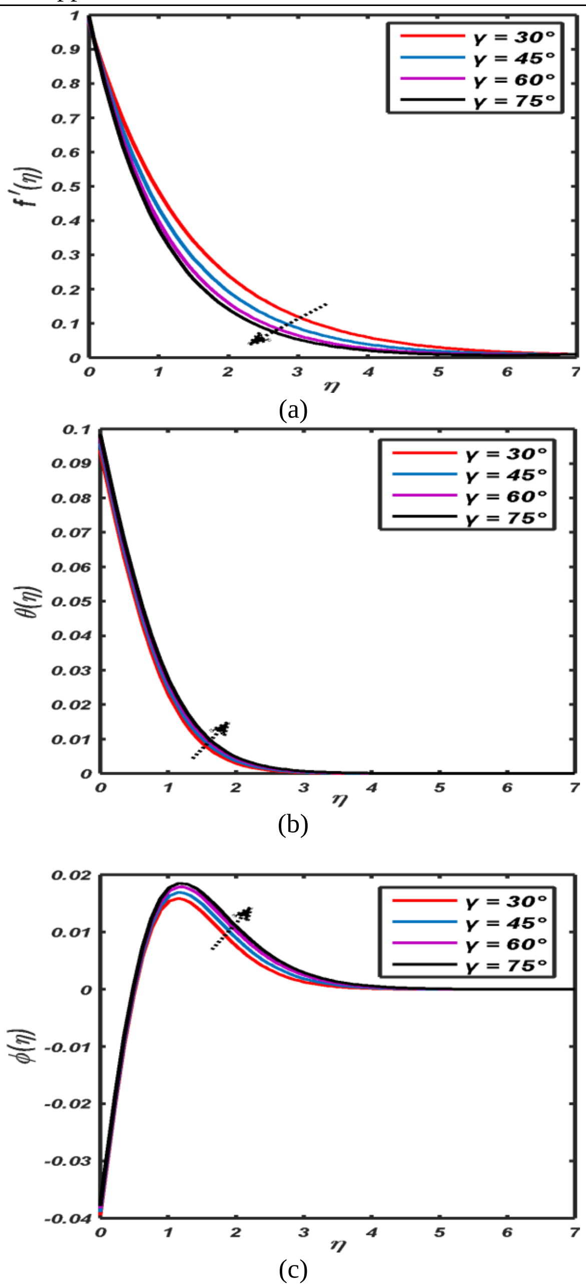

Fig.3: Variation of γ on (a) f', (b) θ, and (c) ϕ profiles.

Figures 4 & 5 illustrate the consequences of Nb & Nt on concentration profile, respectively. Concentration profile upsurges close to the sheet but decreases far away from the sheet for larger values of Nb but reverse effect occurs for larger values of Nt. Brownian motion physically enhances the random spread and dispersion of particles in a fluid, forming a thinner yet denser layer near the boundary, while simultaneously lowering the peak concentration farther from the sheet.

Thermophoresis refers to the migration of particles within a fluid from hotter to cooler regions, decreasing their concentration near hot surfaces while increasing it near cold surfaces, and thereby creating a non-uniform concentration distribution. Figure 6 delineates the consequence of Sc on ϕ profile. It is observed that for increasing values of Sc, concentration upsurges near the sheet but decreases far away from the sheet.

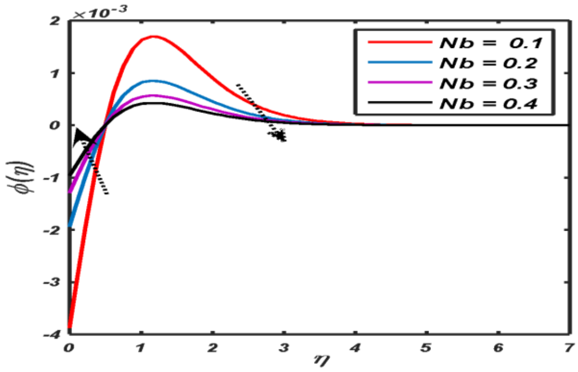

Fig.4: Variation of Nb on ϕ profile.

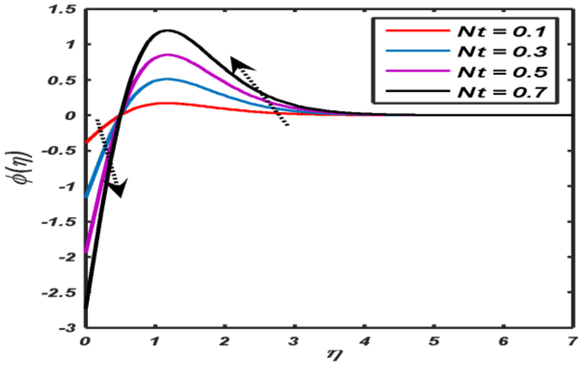

Fig.5: Variation of Nt on ϕ profile.

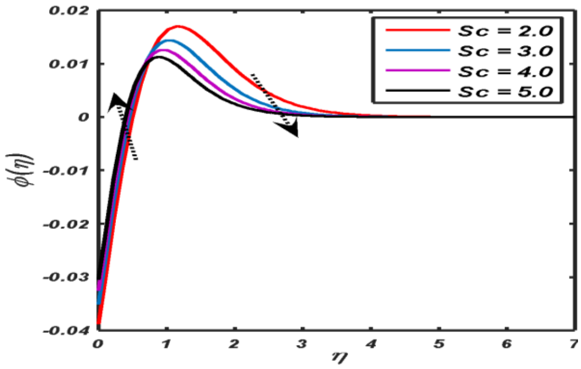

Fig.6: Variation of Sc on ϕ profile.

This behavior arises because the Schmidt number and mass diffusion rate are inversely related; hence, as Sc increases, mass diffusivity decreases, leading to a drop in concentration and a thinner concentration boundary layer farther from the sheet.

Figure 7 illustrates the impact of β on f', and θ profiles. In Figures7 (a), and 7(b), increasing values of Casson parameter causes the velocity to decrease while increasing the temperature inside the boundary layer. The Casson parameter is recognized for generating a resistive force that hinders fluid motion. The increased temperature arises from the resisting force induced by plastic viscosity.

Figure 8 displays the influence of Pr on θ profile. It is observed that temperature reduces for larger values of Pr. Physically, a larger Prandtl number indicates that thermal diffusion occurs slowly than momentum diffusion, resulting in a thinner thermal boundary layer.

Figure 9 depicts the effect of δ_1 on velocity and temperature profiles. In Figs. 9(a) & 9(b), it is observed that the velocity decreases, but the temperature increases, for increasing values of δ_1. Greater slip diminishes the driving effect of the stretched sheet, causing the flow to decelerate as it approaches the free stream. The slip flow phenomenon plays an important role in applications across the petroleum industry and geophysics.

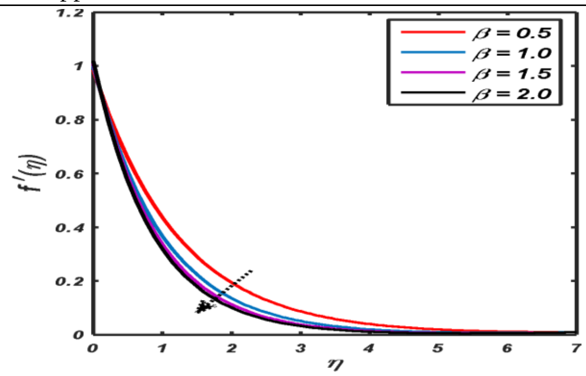

(a)

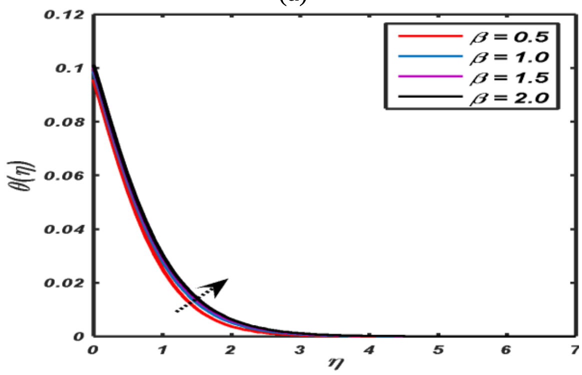

(b)

Fig.7: Variation of β on (a) f', and (b) θ profiles.

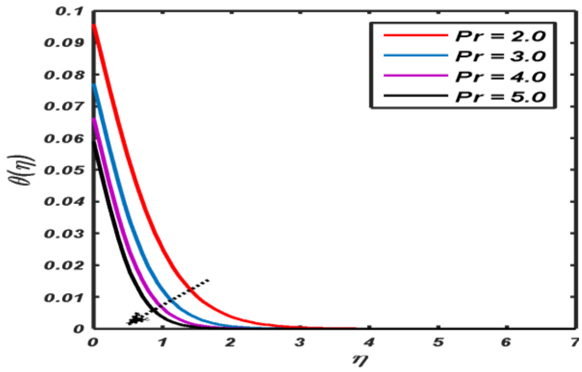

Fig.8: Variation of Pr on θ profile.

Figure 10 shows the impact of A on velocity profile. Velocity increases for increasing values of A which is depicted in Fig. 10. The stretching ratio determines how the sheet's extension is distributed between directions, with higher values intensifying the velocity along the primary stretching direction. Figure 11 displays the impact of δ_2 on velocity and temperature profiles. It is observed that velocity increases but temperature decreases for increasing values of δ_2 which are depicted in Figs. 11(a) and 11(b). A physical derivation is presented to describe the influence of second-order effects on the velocity and temperature jumps at the wall. The analysis employs effective mean free paths for momentum and energy transfer, determined from established values of viscosity and thermal conductivity.

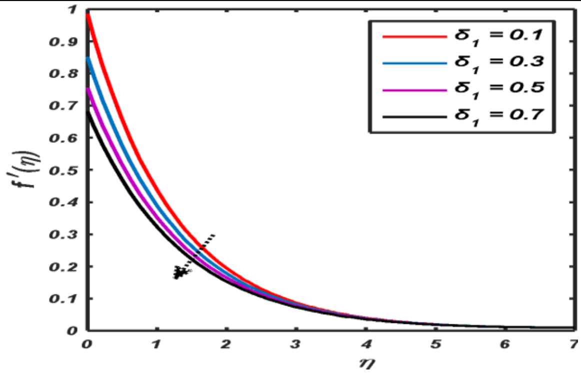

(a)

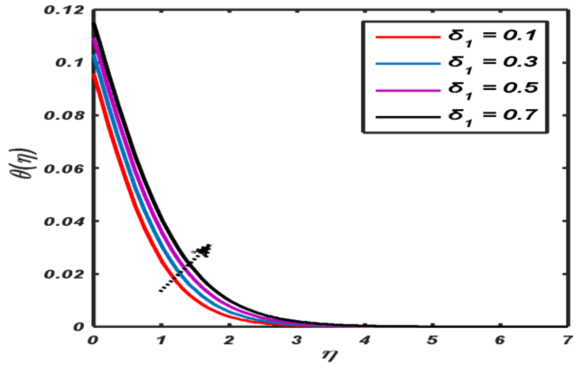

(b)

Fig.9: Variation of δ_1 on (a) f', and (b) θ profiles.

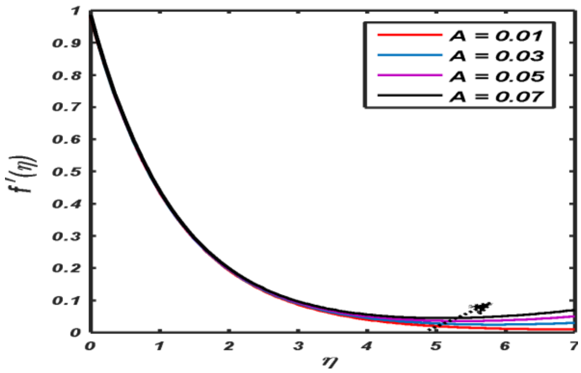

Fig.10: Variation of A on f'profile.

Consequence of Bi on θ profile is illustrated in Fig. 12. Temperature enhances for higher values of Bi. The Biot number determines whether significant temperature variations occur within a body when it is heated or cooled over time through heat flux at its surface.

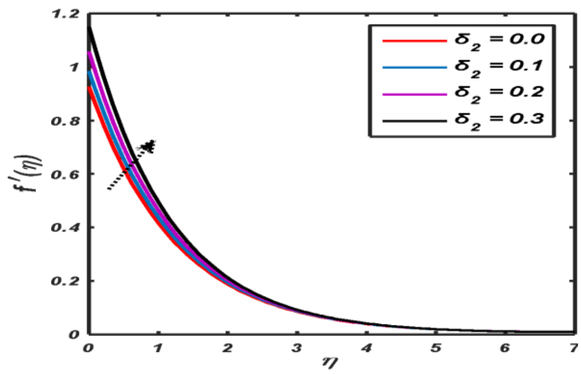

(a)

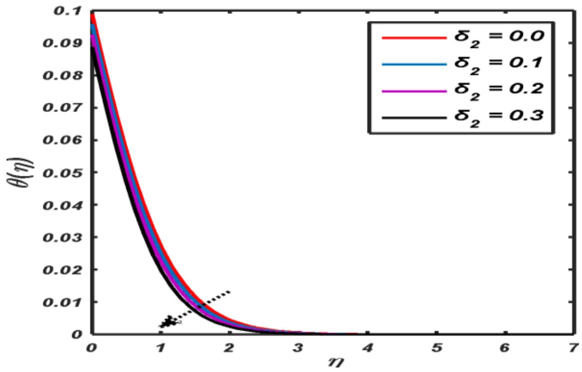

(b)

Fig.11: Variation of δ_2 on (a) f', and (b) θ profiles.

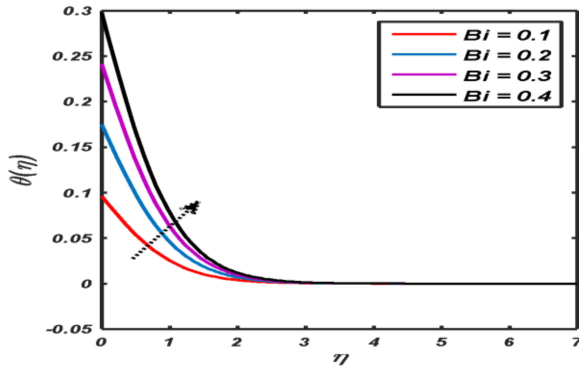

Fig.12: Variation of Bi on θ profile.

5. Conclusion

This study investigated the influences of an inclined magnetic field and higher-order velocity slip on the flow of Casson nanofluid through a stretched sheet, considering Buongiorno model. The current investigation yielded the following conclusions:

- Velocity increases for the changing values of δ_2, A but decreases for larger values of $M, \gamma, \beta, \delta_1$.
- Temperature enhances for increasing values of $M, \gamma, \beta, Bi, \delta_1$ but declines for larger values of Pr, δ_2.
- Concentration upsurges for larger values of M, γ. Also, Concentration increases near the sheet but decreases far away from the sheet for higher values of Nb, Sc. On the other hand, Inverse behavior occurs for Nt.

6. Suggestions for Further Work

Future research can extend the present study to three-dimensional and unsteady Casson nanofluid flows to better represent practical applications.

7. References

[1] Tulapurkara E. G., 2005. Hundred Years of the Boundary Layer. *Sadhana*, 30(04), pp. 499-512.

[2] Sakiadis B. C., 1961. Boundary-Layer Behavior on Continuous Solid Surfaces: II. The Boundary-Layer on a Continuous Flat Surface. *AIChE Journal*, 7, pp. 221–225.

[3] Bakar N. A. A., Zaimi W. M. K. A. W., Hamid R. A., Bidin B., and Ishak A., 2012. Boundary Layer Flow over a Stretching Sheet with a Convective Boundary Condition and Slip Effect. *World Applied Sciences J*ournal, 17, pp. 49-53.

[4] Vinod Y., Raghunatha K. R., Nagappanavar S. N., Nazarova N., Gupta M., and Sangamesh, 2025. Boundary Layer Flow of a Non-Newtonian Fluid over an Exponentially Stretching Sheet with the Presence of a Heat Source/Sink. *Partial Differential. Equations in Applied Math*ematics, 13.

[5] Gladys T., and Reddy G. V. R., 2022. Contributions of Variable Viscosity and Thermal Conductivity on the Dynamics of Non-Newtonian Nanofluids Flow past an Accelerating Vertical Plate. *Partial Differential. Equations in Applied Math*ematics, 5, pp. 100-264.

[6] Priya G., Yaseen Moh., Kumar R. S., and Kumar M., 2022. Heat Transfer in Micropolar Hybrid Nanofluid Flow past a Vertical Plate in the Presence of Thermal Radiation and Suction/Injection Effects. *Partial Differential. Equations in Applied Math*ematics, 5, pp. 100–240.

[7] Casson N., 1959. A Flow Equation for Pigment-Oil Suspensions of the Printing Ink Type. *In Mll, C. C., Ed., Rheology of Disperse Systems, Pergamon Press, Oxford* (pp. 84-104).

[8] Shekar R., Reddy G. J., and Pothanna N., 2025. Influence of Thermal Radiation on MHD Casson Nanofluid Flow over a Non-Linear Stretching Sheet with the Presence of Chemical Reaction. *East European Journal of Phy*sics, 1, pp. 101-111.

[9] Hussain M., Fatima S., and Qayyum M., 2024. Radiative Mixed Convection Flow of Casson Nanofluid through Exponentially Permeable Stretching Sheet with Internal Heat Generation," *Journal of Mathematics*, 2024, 12 pages.

[10] Sekhar P. R., Sreedhar S., Ibrahim S. M., and Kumar P. V., 2023. Radiative Heat Source Fluid Flow of MHD Casson Nanofluid over a Non-Linear Inclined Surface with Soret and Dufour Effects. *CFD Letters*, 15(07), pp. 42-60.

[11] Vijayalaxmi T., and Shankar B., 2016. Effect of Aligned Magnetic Field on Slip Flow of Casson Nanofluid over a Nonlinear Stretching Sheet with Chemical Reaction. *Journal of Nanofluids*, 5, pp. 696–706.

[12] Kosar S., Sagheer M., and Hussain S., 2025. Effect of Inclined Magnetic Field and Chemical Reaction on Casson Fluid Flow over a Stretching Surface with Cattaneo-Christov Double Diffusion. *International Journal of Modern Physics* B, vol. 39, no. 1, April 2025.

[13] Srinivasulu T., and Goud B. S., 2021. Effect of Inclined Magnetic Field on Flow, Heat and Mass Transfer of Williamson Nanofluid over a Stretching Sheet," *Case Studies in Thermal* Engineering, 23.

8. Nomenclature

Symbol	Meaning	Unit
u	Velocity component along the x-axis	(ms^{-1})
v	Velocity component along y-axis	(ms^{-1})
σ	Electrical conductivity	(Sm^{-1})
B_0	Magnetic field strength	($kgs^{-2}A^{-1}$)
υ	Kinematic viscosity	(kgm^{-3})
ρ_f	Density of base fluid	(kgm^{-3})
α	Thermal diffusivity	(m^2s^{-1})
γ	Inclination angle	(Rad.)
D_B	Brownian diffusion	(m^2/s)
D_T	Thermophoresis diffusion	(m^2/s)
l_1	First-order velocity slip	(m/s)
l_2	Second-order velocity slip	(m/s)
k	Thermal conductivity	(W/(m·K))
h_f	Coefficient of heat transfer	($W/(m^2K)$)
β	Casson parameter	Dimensionless
τ	Ratio of nanoparticle effective and base fluid heat capacity	Dimensionless
M	Magnetic field parameter	Dimensionless
Pr	Prandtl number	Dimensionless
Nb	Brownian motion parameter	Dimensionless
Nt	Thermophoresis parameter	Dimensionless
δ_1	First-order velocity slip parameter	Dimensionless
δ_2	Second-order velocity slip parameter	Dimensionless
Bi	Biot number	Dimensionless
A	Stretching ratio parameter	Dimensionless